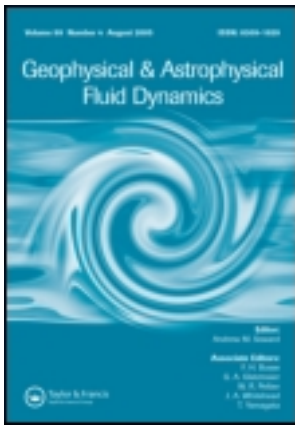


This article was downloaded by: [R.K. Scott]

On: 13 July 2011, At: 12:03

Publisher: Taylor & Francis

Informa Ltd Registered in England and Wales Registered Number: 1072954 Registered office: Mortimer House, 37-41 Mortimer Street, London W1T 3JH, UK



Geophysical & Astrophysical Fluid Dynamics

Publication details, including instructions for authors and subscription information:

<http://www.tandfonline.com/loi/ggaf20>

Polar accumulation of cyclonic vorticity

R.K. Scott ^a

^a School of Mathematics, University of St Andrews, St Andrews KY16 9SS, Scotland

Available online: 13 Jul 2011

To cite this article: R.K. Scott (2011): Polar accumulation of cyclonic vorticity, *Geophysical & Astrophysical Fluid Dynamics*, 105:4-5, 409-420

To link to this article: <http://dx.doi.org/10.1080/03091929.2010.509927>

PLEASE SCROLL DOWN FOR ARTICLE

Full terms and conditions of use: <http://www.tandfonline.com/page/terms-and-conditions>

This article may be used for research, teaching and private study purposes. Any substantial or systematic reproduction, re-distribution, re-selling, loan, sub-licensing, systematic supply or distribution in any form to anyone is expressly forbidden.

The publisher does not give any warranty express or implied or make any representation that the contents will be complete or accurate or up to date. The accuracy of any instructions, formulae and drug doses should be independently verified with primary sources. The publisher shall not be liable for any loss, actions, claims, proceedings, demand or costs or damages whatsoever or howsoever caused arising directly or indirectly in connection with or arising out of the use of this material.

Polar accumulation of cyclonic vorticity

R. K. SCOTT*

School of Mathematics, University of St Andrews,
St Andrews KY16 9SS, Scotland

(Received 26 February 2010; in final form 10 May 2010; first published online 15 September 2010)

The drift of coherent vortices on a background gradient of potential vorticity has been previously studied in the case of uniform gradient. Here an extension is made to the case where the background gradient varies with a radial coordinate in an approximation to the variation of planetary potential vorticity on a rotating sphere. It is found that accumulation of cyclonic vorticity at the pole occurs provided the initial vortex anomaly exceeds the polar value of potential vorticity by approximately 12%. Although polar accumulation becomes slower as the deformation radius decreases, it persists for values as low as about 0.025 of the planetary radius. Polar accumulation of cyclonic vorticity is also found to persist in fully turbulent flows emerging from a large number of coherent vortex anomalies. In this case, a mixed zone in potential vorticity develops in a polar surf zone surrounding the polar cyclone, with a sharp jump at the surf zone edge defining a distinct subpolar jet whose structure depends on the deformation radius. The results are discussed in the context of the coherent polar cyclones and subpolar jets observed on the giant planets.

Keywords: Polar cyclone; Beta-drift; Jets; Potential vorticity staircase

1. Introduction

Recent observations by the space probe Cassini of the polar regions of Saturn revealed the presence of an intense cyclonic (rotating in the same sense as the planetary rotation) coherent vortex situated exactly on each pole (Sánchez-Lavega *et al.* 2006, Fletcher *et al.* 2008). Analysis of thermal emissivity (Fletcher *et al.* 2008) indicated that these structures are deep, spanning several density scale heights from the middle stratosphere down into the troposphere. Their intensity and cloud structure has prompted analogies with terrestrial hurricanes (Dyudina *et al.* 2008, 2009). Convective processes in the atmosphere beneath the cyclones may provide a possible forcing mechanism for their maintenance, although a detailed dynamical picture of the cyclones remains beyond the reach of current observations.

While the polar cyclones may certainly be maintained by external forcing through convective processes and fully three-dimensional motions, it is nevertheless interesting to consider whether simple dynamical processes may be able to explain their presence.

*Email: rks@mcs.st-and.ac.uk

In particular, it is interesting to note that recent single layer shallow water calculations of forced turbulence on the sphere also exhibit strong accumulations of cyclonic vorticity at the poles (see Scott and Polvani (2007), figures 9 and 11, and Scott (2010), figure 1), which suggests the possibility that such structures may arise generically from quasi-two-dimensional dynamics.

The tendency for coherent vortices to drift latitudinally on a background planetary gradient of potential vorticity, so called β -drift, has been known for some time and has been extensively studied in the case of a linear background gradient of potential vorticity (e.g. Reznik 1992, Nycander 1993, Sutyrin *et al.* 1994, Sutyrin and Morel 1997, Lam and Dritschel 2001, Flor and Eames 2002); cyclonic vortices (positive in the northern hemisphere) drift poleward, while anticyclonic vortices drift equatorward. In this simplest case, the final position of such vortices depends on parameters such as the vortex intensity and size relative to the background vorticity and length scales. One aim of this article is to examine to what extent the basic results established for the β -plane case must be modified in the case of spherical polar geometry, for which the planetary vorticity gradient goes to zero at the pole. As discussed below, the spherical geometry fixes a length scale in addition to the Rossby deformation radius (which on the β -plane may be scaled out of the problem) and the ratio of these influences the speed of the drift on the sphere. The spherical geometry also introduces a North–South asymmetry that is absent in the β -plane case.

In the case of isolated vortices drifting on a resting basic state, the drift will naturally favour an accumulation of cyclonic vorticity in polar regions. The situation is further complicated, however, when the background flow is fully turbulent, as is the case on the giant planets themselves. The shallow water experiments of Scott and Polvani (2007) suggest that such drift may still be relevant. The forcing in those experiments is weak but its cumulative effect may eventually result in vortices whose potential vorticity exceeds the planetary value at the pole. Identifying any systematic drift in these fully turbulent flows, however, has so far not been possible. Here we examine the somewhat simpler system of a turbulent flow, freely decaying from an initial condition composed of many coherent vortices. We find that a systematic drift is indeed evident in the fully turbulent flow, despite the strong interactions between vortices.

In the case of fully turbulent flows, the Rossby deformation radius additionally affects the jet structure that emerges near the poles. Comparing this jet structure with those observed on the giant planets suggests that the relevant deformation radius for the polar jets may be larger than the usual estimates based on the structure of coherent vortices such as the Great Red Spot, or on the gravity wave phase speeds observed following the impact of comet Shoemaker-Levy (e.g. Cho *et al.* 2001, Ingersoll *et al.* 2004); that is, the jets may be relatively deep structures. A similar conclusion was made from the forced dissipative shallow water experiments of Scott and Polvani (2007), Scott (2010). The deep nature of these jets has also been noted from observations based on thermal emissivity (Fletcher *et al.* 2008) and has been found in recent three-dimensional general circulation model calculations (Lian and Showman 2008, Schneider and Lui 2009).

The remainder of this article is organized as follows. In section 2, we describe the model equations and geometry used in the experiments, and give a brief discussion of the numerical scheme. In section 3, we examine the vortex drift in the simplest case of isolated vortices to illustrate the North–South asymmetry of the drift and polar accumulation of cyclonic vorticity at various values of vortex intensity and deformation

radius. In section 4, we consider the polar accumulation in the case of a fully turbulent flow arising from many interacting vortices, and examine the region of homogeneous potential vorticity that emerges over the pole due to turbulent mixing. We also briefly consider how undulations of the first circumpolar jet depend on the deformation radius and consider the global structure of the potential vorticity staircase that results from the turbulent mixing. We provide a short summary of the results in section 5.

2. Model equations and numerical scheme

We consider the quasi-geostrophic shallow water equations in a cylindrical domain using a polar coordinate system (r, θ) for a fluid differentially rotating about the cylindrical axis $r = 0$:

$$\frac{\partial q}{\partial t} + J(\psi, q) = 0, \quad (1a)$$

$$(\nabla^2 - L_D^{-2})\psi = q - f(r). \quad (1b)$$

Here, $q(r, \theta, t)$ is the potential vorticity, ψ is the geostrophic streamfunction, $f(r)$ is the radially dependent Coriolis parameter and L_D is the Rossby radius of deformation, measuring the relative importance of stratification and rotation. We make the polar γ -plane approximation, $f = f_0 - \gamma r^2$, where f_0 is the polar value of the Coriolis parameter. This is the polar equivalent to the mid-latitude β -plane. Taking $f_0 = 2\Omega$ and $\gamma = \Omega/2a^2$ gives the first order approximation to the actual variation of the Coriolis parameter near the pole on a spherical planet of radius a rotating with angular velocity Ω . The radial and azimuthal coordinates in the cylindrical domain can be identified with the latitudinal and longitudinal coordinates in spherical geometry near the pole by the correspondence $(r, \theta) \leftrightarrow (a\phi^c, \lambda)$, where ϕ^c is co-latitude and λ is longitude. The approximation is accurate to within about 8% as far as one radian co-latitude from the pole (or an arc distance of one planetary radius) and provides a useful simplified geometry in which to consider polar flows. In a single layer barotropic system, Waugh (1993) used this procedure to represent a variable f on an infinite plane and found good agreement between the planar results of variable f and those obtained with full spherical geometry.

Equations (1a, b) are solved using the Contour Dynamics Semi-Lagrangian scheme (Dritschel and Ambaum 1997, Macaskill *et al.* 2003). The potential vorticity distribution $q(r, \theta, t)$ is assumed to be piecewise uniform, whereby a continuous distribution is represented by a series of small discontinuities across a finite set of contours. Many contours permit high resolution of the potential vorticity distribution, and the efficiencies of this method over the often used pseudo-spectral method for the simulation of freely decaying two-dimensional turbulence were demonstrated recently by Dritschel and Scott (2009). In the simulations described below, 100 contours are used to describe the background potential vorticity field, each with a discontinuity of $\delta q = \Omega/100$, representing potential vorticity values from 2Ω at $r = 0$ to Ω at $r = a$ (corresponding to a latitudinal domain between $\pi/2$ and $\pi/2 - 1$). The horizontal grid used for the PV inversion in (1b) comprises 128 radial and 256 azimuthal grid points;

the PV itself is retained on a grid four times finer. For full details of the numerical scheme, see Macaskill *et al.* (2003).

3. β -drift in polar geometry

We first consider the simplest case of the drift of a single vortex on a background potential vorticity gradient, a situation studied in detail by many authors for the case of the β -plane (e.g. Reznik 1992, Nycander 1993, Sutyrin *et al.* 1994, Sutyrin and Morel 1997, Lam and Dritschel 2001, Flor and Eames 2002, among others). For the case of a vortex patch anomaly of finite radius and intensity, the system is governed by two non-dimensional numbers, a_v/L_D and $q'_v/\beta L_D$, where a_v and q'_v are the radius and intensity of the vorticity anomaly, L_D is the deformation radius and β is the constant background potential vorticity gradient. In a series of high-resolution numerical experiments, Lam and Dritschel (2001) showed that while the longitudinal component of the drift velocity increases monotonically with q'_v (for fixed β and L_D), the latitudinal component peaks at an intermediate value.

On the sphere, the spherical radius, a , introduces an extra length scale, which means that the deformation radius cannot be eliminated by rescaling. In the γ -plane approximation, the above two non-dimensional parameters are replaced by a_v/L_D , $q'_v/\gamma L_D^2$, a/L_D . If the ratio of vortex anomaly radius to spherical radius, and a_v/a , is small, however, then locally the system resembles the β -plane, with β equal to the local gradient of $f(r)$ and we expect all the results of the planar case to apply to the spherical case as long as the vortex does not move over large latitudinal distances. Important differences enter at the global scale because of the variation of f with r . First, since f increases with r , anticyclones drifting to larger r will feel a stronger background potential vorticity gradient than their cyclonic counterparts drifting to smaller r . Destabilizing effects such as Rossby wave radiation are therefore likely to be larger for anticyclones. Similarly, the latitudinal drift will be modified for large vortex excursions in a non-trivial way. Although an anticyclone moves such that it will experience stronger background PV gradient, this is compensated by its perturbation PV, which decreases more rapidly with the latitudinal distance moved from its initial position than that of a cyclone.

Perhaps the most important difference, however, is that the background vorticity gradient vanishes altogether at the pole itself and so any tendency to drift vanishes as this is approached. Quantitatively, the drift of vortices is limited by the intensity of the anomalous vorticity relative to the background planetary rotation, as on the β -plane, since the potential vorticity of the vortex anomaly is conserved following the flow. On the β -plane the vortex may drift up to a maximum distance given by $|q'_v|/\beta$, since at this point the potential vorticity of the vortex will equal that of its surroundings. A trivial extension on the γ -plane gives a maximum drift distance of $|r_v^2 - r^2| = |q'_v/\gamma|$. In particular, a cyclonic vortex would be expected to reach the pole if its potential vorticity exceeds the polar potential vorticity $f_0 = 2\Omega$. Finally, the destabilizing effects arising from Rossby wave radiation also decrease toward the pole, and so coherent cyclones drifting there will be expected to persist on long time scales.

We illustrate the above by a series of numerical experiments from initial conditions consisting of a positive (cyclonic) vortex of intensity q_v at position $r = 0.5$, $\theta = 0$ and a

negative (anticyclonic) vortex of intensity $-q_v$ at position $r=0.5$, $\theta=\pi$, as shown in figure 1 (left). (Here, and in the following, length and time scales are considered to be nondimensionalized with respect to a and Ω .) In each case, the radius of the vortex anomaly is fixed at $a_v=0.02$. This value is constrained, on the one hand, by the numerical requirement that the vortex radius be larger than the spacing between the contours representing the background potential vorticity gradient (here 100 contours equally spaced in r gives a contour spacing of $\delta r=0.01$); on the other hand, for simplicity it is desirable to consider the situation where the variation of the planetary vorticity across the vortex is small. The only remaining free parameters then are the vortex intensity q_v and deformation radius L_D . Here we consider values $q_v-f_0=0, 0.125, 0.25, 0.5, 1$ and $L_D=0.4, 0.1, 0.025$.

As an example, figure 2 shows snapshots of the relative vorticity field for the case $q_v-f_0=1$ and $L_D=0.4$ at times $t=40, 80, 120$. The asymmetry between the cyclone and anticyclone is clear, even at the earliest time, when the cyclone is relatively undisturbed whereas the anticyclone has already lost a significant fraction of its original area. The asymmetry becomes still more pronounced at later times, with the anticyclone eventually destabilizing and breaking up entirely. On the other hand, the cyclone drifts into the weak background potential vorticity gradients near the pole and remains intact there. A similar picture is seen at smaller values of the deformation radius. Figure 3 shows the case $L_D=0.025$: although the evolution is much slower here due to the

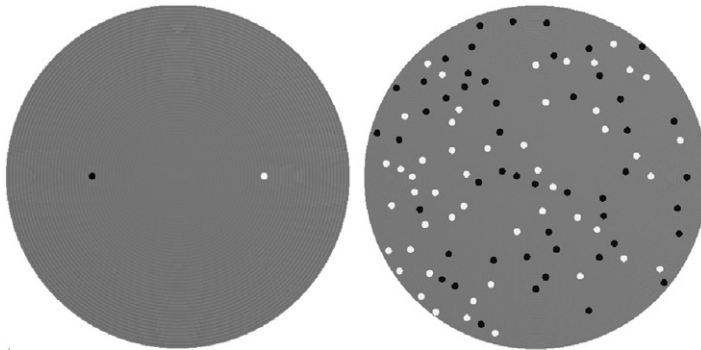


Figure 1. Initial conditions for the experiments described in section 3 (left panel) and section 4 (right panel). Relative vorticity is shown; black and white correspond to negative and positive values, and grey is zero.

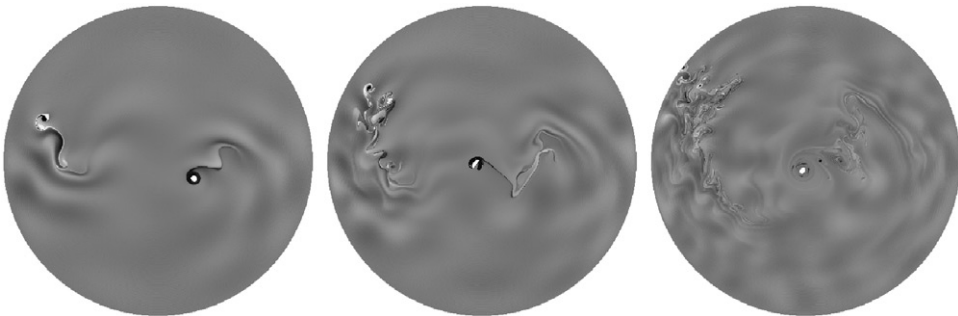


Figure 2. Relative vorticity at $t=40, 80, 160$ (left to right; time, here and elsewhere, in units of background rotation, Ω^{-1}) for the case $L_D=0.4$, $q_v-f_0=1$.



Figure 3. Relative vorticity at $t = 160, 320, 640$ for the case $L_D = 0.025, q_v - f_0 = 1$.

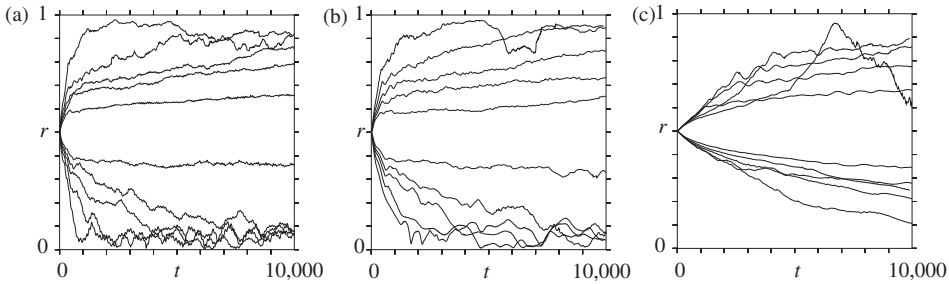


Figure 4. Radial position of the vortex centroid against time, $r(t)$: (a) $L_D = 0.4$, (b) $L_D = 0.1$, (c) $L_D = 0.025$; $|q_v - f_0| = 0, 0.125, 0.25, 0.5, 1$, with larger values of $|q_v - f_0|$ exhibiting stronger drift to $r = 0, 1$.

smallness of L_D , again the anticyclone becomes highly distorted and eventually breaks up. The cyclone drifts poleward but is inhibited by a ring of anticyclonic relative vorticity that accumulates around the core, reducing the effective cyclonicity of the vortex (Korotaev and Fedotov 1994). In some cases this ring can be seen to undergo an instability, similar to that described in Lam and Dritschel (2001), whereby the ring is shed and the cyclone moves further poleward.

The drift of the vortices for various values of $q_v - f_0$ and L_D is summarized in figures 4 and 5. Figure 4 shows the radial positions of the vortex centroids as a function of time $r(t)$. In all cases there is a clear increase in radial drift velocity with increasing q'_v , as expected. However, the cyclone-anticyclone asymmetry is also evident. At both $L_D = 0.4$ and $L_D = 0.1$, whereas all but the weakest cyclones eventually drift to within $r = 0.1$ of the pole, the drift of anticyclones towards $r = 1$ is more dependent on the vortex anomaly. The interpretation is that there is a threshold cyclonic vorticity, above which cyclones will reach the pole. This threshold is slightly greater than the polar vorticity f_0 because of the partial shielding effect arising from entrainment of ambient potential vorticity. At the smallest value of deformation radius $L_D = 0.025$, the drift is still underway at the latest time.

An alternative view can be seen by plotting the trajectories of the vortex centroids in the (r, θ) -plane, as shown in figure 5. Again the polar accumulation of cyclones is clear in all cases. From this figure, it can also be seen that the initial drift angle is relatively insensitive to initial vortex anomaly. For the values considered here, the drift speeds in

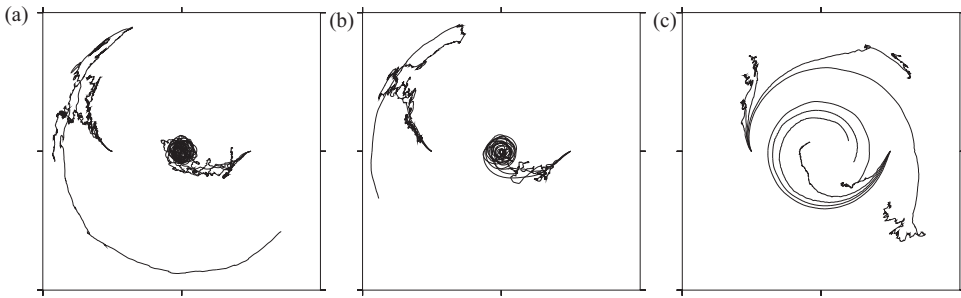


Figure 5. Trajectories of vortex centroids ($r(t)$, $\theta(t)$): (a) $L_D=0.4$, (b) $L_D=0.1$, (c) $L_D=0.025$; $|q_v - f_0| = 0, 0.125, 0.25, 0.5, 1$. $r=0$ is at the centre of the plot.

both the latitudinal and longitudinal directions increase with increasing vortex anomaly (the peak in latitudinal drift speed found by Lam and Dritschel (2001) occurred at larger vortex anomaly than the largest considered here).

4. Polar accumulation in turbulent flow

The case of a single coherent vortex in a resting background atmosphere is a highly simplified situation. To address the question of whether β -drift might account for the polar accumulation of cyclonic vorticity observed on planetary atmospheres, it is more appropriate to consider the evolution of fully turbulent flows. To do so, we consider here an initial condition consisting of a uniform distribution of an equal number of positive and negative coherent vortices. For simplicity, and to minimize the number of additional parameters, we choose vortices all having the same area $a_v=0.02$ (as for the isolated vortices in the previous section), and anomalous intensity $q'_v = q_v - f = \pm 0.25\Omega$ (i.e. a potential vorticity differing from the local background value by 0.25Ω). The main parameter governing the turbulent intensity of the subsequent evolution is the area fraction A_f of the domain covered by vortices. Here we take $A_f=0.04$, for which the area of the polar mixed zone in the final state is roughly consistent with the location of the polar-most jets on the giant planets, as discussed further below. The initial relative vorticity corresponding to these values is shown in figure 1 (right).

As an example, the evolution of the case with $L_D=0.4$ is shown in figure 6, which shows the relative vorticity at early, intermediate and late times. At early time, $t=100$, a highly turbulent flow field has emerged from the interactions of the initial vortex population. The turbulent intensity is strongest away from the pole, where advection of background planetary vorticity contributes to the relative vorticity field. Near the pole, already at early times, the accumulation of cyclonic vorticity (white) is clear. By $t=400$ the turbulent cascade of enstrophy to smaller scales is visible throughout the domain, with the exception of the coherent cyclone near the pole, which retains most of its area as time progresses. By the end of the calculation at $t=10,000$ the cascade of enstrophy has proceeded further everywhere throughout the domain, while the coherent cyclone remains intact and settles into a stable position at the pole.

During the intermediate evolution to this final state, a prolonged period exists where the polar cyclone is well-developed but not situated exactly at the pole. The weak

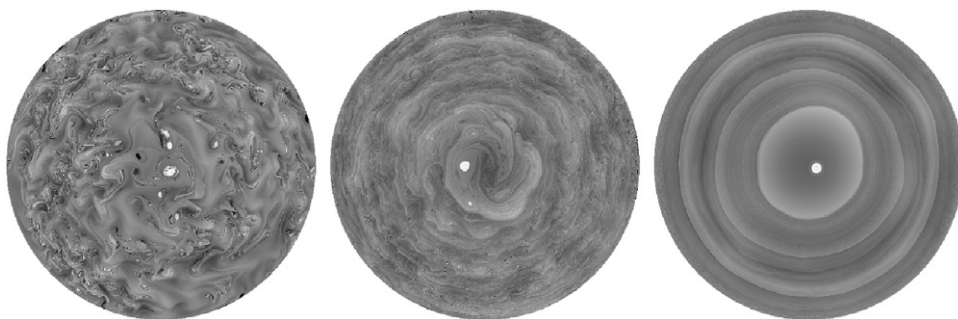


Figure 6. Relative vorticity at $t=100, 400, 10,000$ for the case $L_D=0.4, A_f=0.004, q_v=0.25$.

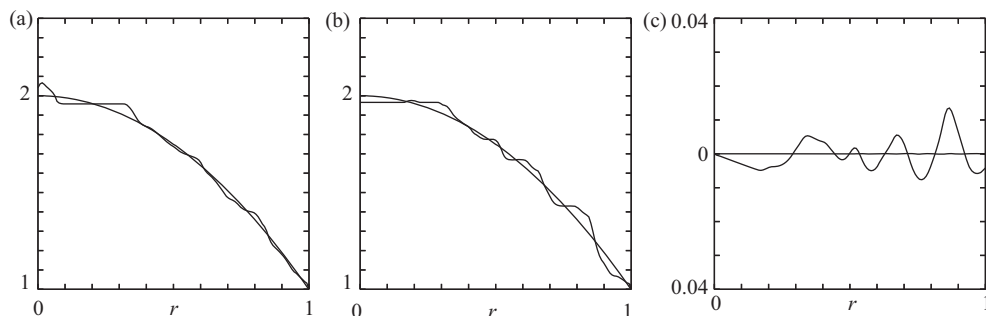


Figure 7. (a) Azimuthally averaged potential vorticity at $t=10,000$ for the case $L_D=0.4$; (b) and (c) azimuthally averaged potential vorticity and azimuthal velocity, respectively, at $t=100,000$ for the $L_D=0.05$.

planetary potential vorticity gradients near the pole provide a weak constraint to its location. Further, its off-pole location leads to efficient chaotic mixing of planetary vorticity over the polar region (middle panel of figure 6) and leads quickly to a potential vorticity profile that is perfectly homogenized over this region. The width of this region increases both with the area fraction A_f and initial potential vorticity anomaly q_v , both of which increase the total energy of the flow (not shown). The dependence is consistent with relations obtained between jet spacing and jet strength in the simple zonally symmetric configurations considered by Dunkerton and Scott (2008) and Dritschel and McIntyre (2008) on the sphere and β -plane, respectively.

The azimuthally averaged potential vorticity for the above case is shown in figure 7(a), demonstrating that the potential vorticity is perfectly mixed across the pole between the cyclone near $r=0$ and approximately $r=0.35$. The perfect homogenization of potential vorticity in this region illustrates how closely the limiting azimuthally symmetric case and perfect staircase can be approached in a fully turbulent situation. Mixing is slower farther from $r=0$, with only partial mixing of the azimuthally averaged potential vorticity in this case. Other cases, however, exhibit more complete mixing at later times. The complexity of the flows at large L_D makes very long time integrations prohibitively time-consuming. However at intermediate to small L_D , very long integrations were possible: in these cases it appears, qualitatively speaking, that

enstrophy production takes place on a longer time-scale (that associated with the large-scale dynamics, which typically increases as L_D decreases) than enstrophy dissipation, which is governed by local small-scale potential vorticity fluctuations (here the same across calculations). Figure 7(b) shows the azimuthally averaged potential vorticity at time $t = 100,000$ for the case of $L_D = 0.05$. By this time, almost all the filamentary turbulence has been dissipated, leaving behind a well-defined staircase structure consisting of almost perfectly mixed zones between narrow regions of strong potential vorticity gradients. The corresponding azimuthally averaged azimuthal velocity is shown in figure 7(c) and consists of the usual sharp and narrow jets coinciding with the jumps in the potential vorticity.

The steep potential vorticity jumps shown in figure 7(b) are noteworthy in view of the difficulty that previous studies of freely decaying turbulence have had in producing similar structures. It is likely that this difficulty is due to finite Reynolds number effects. Calculations using pseudo-spectral or other traditional methods are unlikely to be able to conserve energy over sufficiently long times for staircase formation to become manifest. Here, on the other hand, the effectively inviscid nature of the Lagrangian contour representation means that energy dissipation is very weak, even over the long time-scales under consideration. By essentially inviscid is meant the total absence of diffusion across potential vorticity jumps, such as those that form in the staircase; dissipation does occur, but only weakly through the removal of filamentary structures below a certain scale. For a detailed comparison between the contour dynamical and pseudo-spectral methods in representing freely-decaying two-dimensional turbulence see Dritschel and Scott (2009). Although the staircase structure emerging in figure 7(b) can also be obtained on the β -plane (again provided suitably non-dissipative numerical methods are used – work to be published in the future), we note again that the enhanced stirring by the polar cyclone in the present case leads to particularly efficient mixing over the polar cap.

The mixed zone in the polar regions, and the structure of the first complete jet from the pole, are interesting in other aspects. As can be seen in figure 8, the structure of the first jet varies significantly with L_D . For $L_D \gtrsim 0.2$ the potential vorticity distribution in the polar regions is largely azimuthally symmetric; however, at smaller L_D the azimuthal structure becomes increasingly distorted. In particular, at $L_D = 0.025$, there are large undulations of the first polar jet resulting from the shorter range nature of the Helmholtz operator governing the potential vorticity inversion (e.g. McIntyre 2008, for a recent discussion). A similar pattern was noticed in the forced-dissipative shallow water calculations of Scott and Polvani (2007) (see figure 9 therein). The present calculations illustrate that the undulations do not only arise in the presence of forcing, but are a persistent feature of the small deformation radius. (The calculations at the three lowest values of L_D were continued for a longer time, with only slight changes in the qualitative structure of the first polar jets.) Finally, we note again that in all cases the persistence of the cyclonic vortex at the pole is a robust feature.

5. Conclusions

Provided the latitudinal migration of coherent vortices is small relative to the planetary radius, the drift induced by the interaction of vortex anomalies with the background

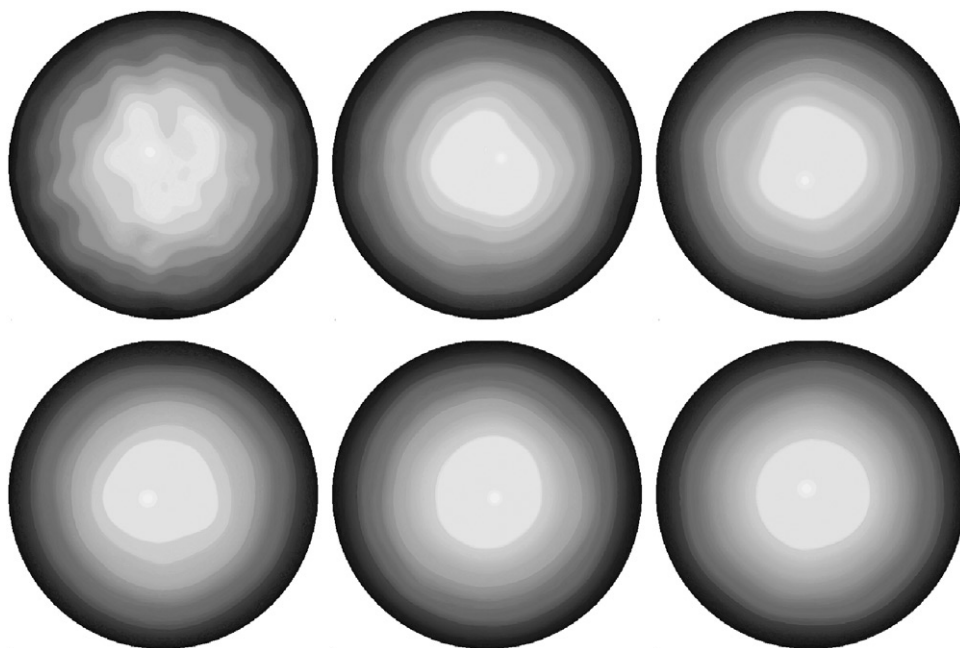


Figure 8. Potential vorticity at $t = 100,00$ for the cases $L_D = 0.025, 0.05, 0.1, 0.2, 0.4, 0.8$, $A_T = 0.004$ (left to right, top to bottom) $q'_v = 0.25$.

planetary potential vorticity may be well-approximated by the β -plane system. However, when the vortices drift over distances comparable to the planetary radius asymmetries arise from the non-uniformity of the planetary vorticity gradient. The asymmetry first appears in the tendency for southward drifting anticyclones to be destabilized by the increased planetary vorticity gradient. Northward drifting cyclones, on the other hand, may approach the weaker planetary vorticity gradients at the pole without becoming significantly distorted. It was found that provided the potential vorticity anomaly exceeds the polar value by 0.25, i.e. $1/8$ of the polar potential vorticity, then the vortex typically drifts to within $r = 0.1$ of the pole, in which region it then remains.

The polar drift of cyclonic vortices persists even when the initial configuration comprises many vortices and the subsequent flow evolves turbulently. In this case the turbulent mixing results in a homogeneous region of potential vorticity surrounding the polar cyclone that emerges. Mixing is more efficient in this region because of the weakness of potential vorticity gradients. It is achieved partially by the stirring induced by the polar cyclone itself, which typically sits slightly displaced from the pole and precesses about it, giving rise to a chaotic mixing type flow in the vicinity. Mixing at larger r also takes place, but on longer time scales. At the edge of the well-mixed polar surf zone the abrupt jump in potential vorticity to the local planetary value is associated with a strong zonal jet.

The tendency found in the above calculations, particularly those at small deformation radius, for the polar cyclones to precess around the pole is not observed in the polar regions of Jupiter and Saturn. Of course, on the planets, various other effects such as radiative cooling over the pole, or forcing from below, may act to further constrain the

motion into zonal symmetry, whereas in the above calculations no such forces are present other than the dynamical effect of the planetary potential vorticity. The same applies to the subpolar jet that occurs at the edge of the polar surf zone, the corresponding jets on the planets appearing very zonal (e.g. Fletcher *et al.* 2008). While it is conceivable that weak zonally symmetric forcing could result in strong zonal alignment of the planetary jets, even at small deformation radius, an alternative explanation, consistent with the increase in zonal undulations with decreasing deformation radius found above, is simply that the planetary jets may be relatively deep structures.

Acknowledgement

This work was supported by the National Science Foundation under grant AGS-0827210.

References

- Cho, J.Y.-K., de la Torre Jurez, M., Ingersoll, A.P. and Dritschel, D.G., A high-resolution, three-dimensional model of Jupiter's Great Red Spot. *J. Geophys. Res.* 2001, **106**, 5099–5105.
- Dritschel, D.G. and Ambaum, M.H.P., A contour-advective semi-Lagrangian numerical algorithm for simulating fine-scale conservative dynamical fields. *Q. J. R. Meteorol. Soc.* 1997, **123**, 1097–1130.
- Dritschel, D.G. and McIntyre, M.E., Multiple jets as PV staircases: the Phillips effect and the resilience of eddy-transport barriers. *J. Atmos. Sci.* 2008, **65**, 855–874.
- Dritschel, D.G. and Scott, R.K., On the simulation of nearly inviscid two-dimensional turbulence. *J. Comp. Phys.* 2009, **228**, 2707–2711.
- Dunkerton, T.J. and Scott, R.K., A barotropic model of the angular momentum conserving potential vorticity staircase in spherical geometry. *J. Atmos. Sci.* 2008, **65**, 1105–1136.
- Dyudina, U.A., Ingersoll, A.P., Ewald, S.P., Vasavada, A.R., West, R.A., Del Genio, A.D., Barbara, J.M., Porco, C.C., Achterberg, R.K., Flasar, F.M. Simon-Miller, A.A. and Fletcher, L.N., Dynamics of Saturn's South Polar Vortex. *Science* 2008, **319**, 1801.
- Dyudina, U.A., Ingersoll, A.P., Ewald, S.P., Vasavada, A.R., West, R.A., Del Genio, A.D., Barbara, J.M., Porco, C.C., Achterberg, R.K., Flasar, F.M. Simon-Miller, A.A. and Fletcher, L.N., Saturn's south polar vortex compared to other large vortices in the Solar System. *Icarus* 2009, **202**, 240–248.
- Fletcher, L.N., Irwin, P.G.J., Orton, G.S., Teanby, N.A., Achterberg, R.K., Bjoraker, G.L., Read, P.L., Simon-Miller, A.A., Howett, C., de Kok, R., Bowles, N., Calcutt, S.B., Hesman, B. and Flasar, F.M., Temperature and composition of Saturn's polar hot spots and hexagon. *Science* 2008, **319**, 79–81.
- Flor, J.-B. and Eames, I., Dynamics of monopolar vortices on a topographic beta-plane. *J. Fluid Mech.* 2002, **456**, 353–376.
- Ingersoll, A.P., Dowling, T.E., Gierasch, P.J., Orton, G.S., Read, P.L., Sanchez-Lavega, A., Showman, A.P., Simon-Miller, A.A. and Vasavada, A.R., Dynamics of Jupiter's atmosphere. In *Jupiter: the Planet, Satellites, and Magnetosphere*, pp. 105–128, 2004 (Cambridge University Press: Cambridge).
- Korotaev, G.R. and Fedotov, A.R., Dynamics of an isolated barotropic eddy on a beta-plane. *J. Fluid Mech.* 1994, **264**, 277–301.
- Lam, J.S.-L. and Dritschel, D.G., On the beta-drift of an initially circular vortex patch. *J. Fluid Mech.* 2001, **436**, 107–129.
- Lian, Y. and Showman, A.P., Deep jets on gas-giant planets. *Icarus* 2008, **194**, 597–615.
- Macaskill, C., Padden, W. and Dritschel, D., The CASL algorithm for quasi-geostrophic flow in a cylinder. *J. Comput. Phys.* 2003, **188**, 232–251.
- McIntyre, M.E., Potential-vorticity inversion and the wave-turbulence jigsaw: some recent clarifications. *Adv. Geosci.* 2008, **15**, 47–56.
- Nycander, J., The difference between monopole vortices in planetary flows and laboratory experiments. *J. Fluid Mech.* 1993, **254**, 561–577.
- Reznik, G.M., Dynamics of singular vortices on a beta-plane. *J. Fluid Mech.* 1992, **240**, 405–432.

- Sánchez-Lavega, A., Hueso, R., Pérez-Hoyos, S. and Rojas, J.F., A strong vortex in Saturn's south pole. *Icarus* 2006, **184**, 524–531.
- Schneider, T. and Lui, J., Formation of jets and equatorial superrotation on Jupiter. *J. Atmos. Sci.* 2009, **66**, 579–601.
- Scott, R.K., The structure of zonal jets in shallow water turbulence on the sphere. In *Proceedings of the IUTAM symposium on Rotating Stratified Turbulence*, 2010, In press.
- Scott, R.K. and Polvani, L.M., Forced-dissipative shallow water turbulence on the sphere and the atmospheric circulation of the gas planets. *J. Atmos. Sci.* 2007, **64**, 3158–3176.
- Sutyryn, G.G., Hesthaven, J.S., Lynov, J.P. and Rasmussen, J.J., Dynamical properties of vortical structures on the beta-plane. *J. Fluid Mech.* 1994, **268**, 103–131.
- Sutyryn, G.G. and Morel, Y.G., Intense vortex motion in a stratified fluid on the beta-plane: an analytical theory and its validation. *J. Fluid Mech.* 1997, **336**, 203–220.
- Waugh, D.W., Contour simulations of a forced polar vortex. *J. Atmos. Sci.* 1993, **50**, 714–730.